JOURNAL OF SPACECRAFT AND ROCKETS
Vol. 46, No. 5, September–October 2009

Numerical Study on Choked Flow over Grid-Fin Configurations

Jinsheng Cai*
Northwest Polytechnical University, 710072 Xi'an, People's Republic of China

DOI: 10.2514/1.41442

An improved configuration, which we term a swept-back grid fin, is proposed in the present study to reduce the detrimental effects of high drag caused by the flow choking within the transonic regime. Viscous computational fluid dynamics simulations were performed to investigate flows over a missile with baseline and swept-back grid fins under supersonic and transonic conditions at zero incidence. The computed drag coefficients for the baseline missile agree well with those in the literature. Our numerical results indicate that flow choking can be reduced by using the swept-back grid fin. As a result, the drag coefficient on the fins is decreased by approximately 13% for all the Mach numbers investigated in the present study.

Nomenclature

C_D	=	drag coefficient on the whole missile
C_{Df}	=	drag coefficient on the grid fin only
C_p	=	pressure coefficient
c	=	chord length for a lattice grid-fin configuration
D	=	diameter of the cylinder
h	=	height for a lattice grid-fin configuration
Ma	=	calculated Mach number
$M\infty$	=	freestream Mach number
Re_D	=	Reynolds number, $U_\infty D/\nu_\infty$
s	=	span for a lattice grid-fin configuration
t	=	thickness of the cell spar for a lattice grid-fin configuration
U_∞	=	freestream velocity
α	=	swept-back angle
ν	=	kinematic viscosity

I. Introduction

A GRID fin, also termed a lattice grid fin, is a less conventional aerodynamic control device consisting of an outer frame with an internal intersecting grid made up of cells with small chord lengths. Unlike conventional fins that are aligned parallel to the direction of the airflow, grid fins are arranged perpendicular to the flow, allowing the oncoming air to pass through the lattice grid cells.

The primary advantage of grid fins is that they have a much shorter chord length than conventional planar fins. As a result, they generate smaller hinge moments, which require smaller actuators to rotate them in a high-speed flow. The small chord length of grid fins also makes them less likely to stall at high angles of attack. This resistance to stall increases the control effectiveness of grid fins compared with conventional planar fins. Because of their unique shape and small chord length, grid fins can be conveniently folded against the body so as to make them easier to store or transport. For this reason, grid fins have attracted much attention in recent years.

The first investigation of grid-fin aerodynamics was carried out by Belotserkovskiy et al. [1] using a theoretical method that relied mainly on empirical formulas. Some analytical work has also been conducted using the vortex-lattice-type approach in the subsonic regime [2]. More recently, Theerthamalai and Nagarathinam [3] developed an aerodynamic prediction method for the estimation of the aerodynamic characteristics of grid-fin configurations at supersonic Mach numbers. The shock and expansion relations and the interactions between the shock and expansion waves were used to predict the pressure distribution inside each grid-fin cell.

Washington et al. [4] conducted wind-tunnel experiments to study the effects of fin curvature and leading-edge sweep back on the aerodynamic characteristics at several subsonic and supersonic Mach numbers and different angles of attack. The balance data indicated that "fin curvature has a small effect on fin normal force, hinge moment, and bending moment." Miller and Washington [5] extended the experiments to study the effects on drag of the outer frame cross-sectional shape and the cell spar thickness. Their findings indicated that a simple shaping of the frame cross section, a reduction of the cell spar thickness, or a combination of both can yield considerably lower drag levels with minimal impact on the grid-fin lift and other aerodynamic properties. Ballistic experiments conducted by Abate et al. [6] at the U.S. Air Force's Aeroballistic Research Facility (ARF) focused on the overall aerodynamic performance of missiles with grid fins in the subsonic and transonic regimes. They found a critical transonic Mach number at which normal shocks and choked flow are believed to have formed within some of the cells. At this Mach number, dynamic instabilities are visible together with rapid fluctuations in the normal force. These studies relied mainly on force and moment measurements from individual fins or from the whole missile. No attempt was made to resolve in detail the flow characteristics inside and around the lattice cells or to optimize the cross section of their walls.

Besides theoretical and experimental studies, computational fluid dynamics (CFD) analysis has been used to investigate the aerodynamic characteristics of grid-fin configurations. Chen et al. [7] conducted numerical investigations of a missile configuration with grid fins by using the NPARC code of NASA. The issue of the optimum grid-fin size, in terms of both the panel thickness and the frontal shape, was addressed. Lin et al. [8] performed computations of turbulent flows past a grid fin alone and fin-body combinations at Mach numbers of 2.5 and 0.7. The computations provided detailed flowfields, including Mach number contours, pressure contours, streamline patterns, and the integrated aerodynamic coefficients. DeSpirito and Sahu [9] and DeSpirito et al. [10] conducted CFD studies on grid fins using the commercial CFD code FLUENT, which presented the first known published viscous CFD computations of grid fins. The simulations successfully predicted the flow structures around the fin in the separated flow region at higher angles of attack. The objective was to investigate the advantages grid fins offered over conventional controls when employed on highly maneuverable missiles. DeSpirito et al. [11] also performed viscous CFD calculations to predict the aerodynamic coefficients and flowfield around a generic canard-controlled missile with planar and grid tail fins in supersonic flow. The CFD results showed the advantages of grid fins in alleviating roll control issues related to canard trailing vortex-fin interactions. Hughson et al. [12] conducted CFD studies to investigate the flowfields over the missile–grid-fin configuration tested by

Received 7 October 2008; revision received 4 June 2009; accepted for publication 18 June 2009. Copyright © 2009 by the American Institute of Aeronautics and Astronautics, Inc. All rights reserved. Copies of this paper may be made for personal or internal use, on condition that the copier pay the $10.00 per-copy fee to the Copyright Clearance Center, Inc., 222 Rosewood Drive, Danvers, MA 01923; include the code 0022-4650/09 and $10.00 in correspondence with the CCC.

*Professor, National Key Laboratory of Aerodynamic Design and Research; caijsh@nwpu.edu.cn.

Abate et al. [6]. The CFD results showed the presence of choked flow within the cells and the formation of a normal shock behind the grid fin at transonic Mach numbers.

An important aerodynamic feature of grid fins is their drag dependence [5,6] on the speed of the missile. At low subsonic speeds, the drag and control effectiveness of the grid fin are almost similar to a conventional fin, because the thin shape of the lattice walls creates minimal disturbance to the passage of air flow. However, the same behavior does not hold true in the transonic regime. The flow chokes within the cells, reducing the flow rate through the fin, and the lattice effectively acts as an obstacle to the flow, resulting in a significant increase in drag. At higher speeds, the normal shock is swallowed and the shock passes through the structure without intersecting it. In this regime, the control effectiveness of grid fins is superior.

Thus, the main objective of the present CFD study is to find a method of overcoming the high drag of the grid fin in the transonic flow regime. An amended configuration, a swept-back grid fin, is proposed to reduce the transonic choking without compromising the control effectiveness of the grid fin. The physics of the shock interaction and choking behavior within the cells of both normal and swept-back grid fins are also examined under both transonic and supersonic conditions.

II. Numerical Approach

A. Geometry

The geometry investigated by Abate et al. [6] and Hughson et al. [12] is selected as the baseline, which consists of a 3-caliber tangent ogive nose and a 13-caliber-long cylindrical afterbody with four grid fins mounted in a cruciform orientation, as shown in Fig. 1a. The pitch axis of the grid fins is located 1.5 calibers from the rear of the cylinder. The front view of the baseline grid-fin structure is shown in Fig. 1b. The grid fin has rectangular-shaped outer frames, with a span (s), height (h), and chord (c) of 0.75, 0.333, and 0.118 calibers, respectively. The cell spar thickness (t) is 0.007 calibers, and the body caliber, or diameter (D), is 1 in.

To reduce choking, the framework of grid cells of the baseline structure is swept back along the chord direction with the same projected structure and dimensions as shown in Figs. 1b. Figures 1c and 1d show the top view of the baseline and swept-back grid fin, respectively. In the present study, the swept-back angle (α) is 30 deg. The swept-back grid fins are also mounted at the same position and orientation relative to the body compared with the baseline grid fin. The swept-back angle of 30 deg may be not the optimum one, but this angle of swept back was selected in the present study because it is a critical angle that can exactly make the front boundary of the swept-back framework just touch the rear boundary of the baseline framework (see Figs. 1c and 1d).

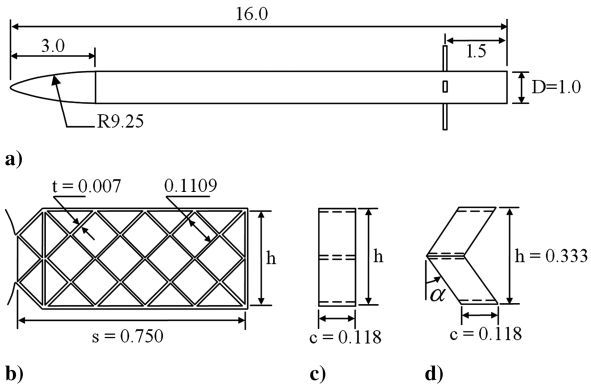

Fig. 1 Schematic of the configurations: a) side view of ogive cylinder and fins, b) front view of grid fin, c) top view of baseline grid fin, d) top view of swept-back grid fin.

B. Numerical Method and Flow Solver

The computation of flow within the cells of the grid fins is a challenging task, especially because the interaction of the shock waves formed at the blunt leading edges of each cell spar produces complex flow features. In the present study, three-dimensional Navier–Stokes equations coupled with a turbulence model are used to simulate the turbulence field. In this section, the mathematical model and the numerical solutions of the model are outlined briefly.

The governing equations for three-dimensional unsteady, compressible, turbulent flow are expressed as follows:

$$\frac{\partial \rho}{\partial t} + \frac{\partial}{\partial x_j}(\rho u_j) = 0 \tag{1}$$

$$\frac{\partial}{\partial t}(\rho u_i) + \frac{\partial}{\partial x_j}(\rho u_j u_i) = -\frac{\partial p}{\partial x_i} + \frac{\partial \hat{\tau}_{ji}}{\partial x_j} \tag{2}$$

$$\frac{\partial}{\partial t}(\rho E) + \frac{\partial}{\partial x_j}(\rho u_j H) = \frac{\partial}{\partial x_j}\left[u_i \hat{\tau}_{ij} + (\mu + \sigma^* \mu_T)\frac{\partial k}{\partial x_j} - q_j\right] \tag{3}$$

where t is the time, x_i is the position vector, ρ is the density, u_i is the velocity vector, p is the pressure, and μ is the dynamic molecular viscosity. The total energy and enthalpy are $E = e + k + u_i u_i/2$ and $H = h + k + u_i u_i/2$, respectively, with $h = e + p/\rho$ and $e = p/[(\gamma - 1)\rho]$. The term γ is the ratio of specific heats. Other quantities are defined in the following equations:

$$\mu_T = \rho \nu_t \tag{4}$$

$$\sigma_{ij} = \frac{1}{2}\left(\frac{\partial u_i}{\partial x_j} + \frac{\partial u_j}{\partial x_i}\right) \tag{5}$$

$$\tau_{ij} = 2\mu_T\left(S_{ij} - \frac{1}{3}\frac{\partial u_k}{\partial x_k}\delta_{ij}\right) - \frac{2}{3}\rho k \delta_{ij} \tag{6}$$

$$\hat{\tau}_{ij} = 2\mu\left(S_{ij} - \frac{1}{3}\frac{\partial u_k}{\partial x_k}\delta_{ij}\right) + \tau_{ij} \tag{7}$$

$$q_j = -\left(\frac{\mu}{Pr_L} + \frac{\mu_T}{Pr_T}\right)\frac{\partial h}{\partial x_j} \tag{8}$$

where δ_{ij} indicates the Kronecker delta.

The commercial CFD software FLUENT was chosen as the flow solver for the three-dimensional Reynolds-averaged Navier–Stokes equations to model the flow phenomena. The governing equations were solved by using a finite volume method with an unstructured grid. The Spalart–Allmaras one-equation turbulence model was used for all simulations. A second-order, upwind discretization was also employed for all flow variables, including the turbulent viscosity. A density-based implicit solver was adopted for the cases involving high-speed compressible flow. Parallel computing was carried out by eight processors to speed up the computation. A reduction in the maximum residuals by at least 3 orders of magnitude was used as the global convergence criterion for all simulations. The axial force coefficient was also tracked to ensure that it was converged. Actually, the axial force coefficient converged even faster than the global convergence criterion.

C. Computational Mesh

The most challenging aspect of the CFD simulations of the flow over a missile with grid fins is to create a mesh of high quality. Because of their complicated geometry, the generation of the structured grid for the fins is highly resource intensive and requires

experience. As such, in the present study, GAMBIT, part of the CFD software FLUENT suite, was used to generate the unstructured grid. To take advantage of model symmetry at a zero angle of attack, only one-eighth of the missile (with a grid fin attached) was chosen as the calculation domain in the current CFD study.

Using the wall function in FLUENT, a boundary-layer mesh was used near the missile body and fin surfaces. The spacing between the first grid point and the surface is $0.001D$, with a growth factor of 1.2 and at least nine points distributed within the boundary layer corresponding to the Reynolds number used by the free flight test of Abate et al. [6]. To enhance the mesh quality, the whole computational domain is divided into three sections comprising, respectively, the fin, the transition section, and the remaining section.

Figures 2a and 2b show the enlarged view of the grid of the front and wake regions near the body on the symmetry surface, respectively, and Figs. 2c and 2d show the enlarged view of the grid on the slices of the fin front surface and symmetry surface, respectively. An unstructured triangular mesh was used for the fin section (Fig. 2a). Grids within the fin section are highly clustered to the cell surface as well as the leading and trailing edge of each cell spar. Three transitional sections were located on the top of, before, and after the fin section, respectively. Within these transitional sections, the very fine mesh in the fin can be gradually merged into the coarse mesh in the remaining section, thus significantly reducing the total grid number for the whole computational domain. As seen in Fig. 2b, a T-grid type was used within these transitional sections. The advantage of this type of grid is the unrestricted usage of grid number and grid type for different surfaces, whereas the disadvantage is that the volume mesh depends strongly on the mesh quality of each surface. In the remaining section, which consists mainly of the ogive cylinder body, a structured grid was used, as shown in Figs. 2a and 2b. The upstream and downstream boundaries are located 12 calibers away from the nose and tail of the cylinder body and 16 calibers radially from the cylinder surface.

Compared with the body length of 16 calibers, the present outer boundaries were located only one body length away or less, which is much shorter for computations at a nonzero angle of attack, for which cases the outer boundaries were usually put at least several body-lengths away [11]. However, as the main focus of the present study was to investigate the flow choking physics, only cases with a zero angle attack were considered. Very fine mesh is necessary in the grid-fin region to capture the complicated flow phenomena near the grid-fin cells; the total mesh elements can be saved with not so large a computation domain when the specific far-field boundary conditions on the outer boundaries are used to ensure the accuracy of the transonic flow computation.

Grid-independence has been studied during the computations by checking the difference of total drag (including base drag) for coarse and fine grids. Compared with a previous study [12], the results showed that the grid used in the current study can simulate the flow phenomena accurately. Only a one-eighth flow domain covered with 1 million grid cells was considered here by taking advantage of the flow symmetry at a zero angle of attack.

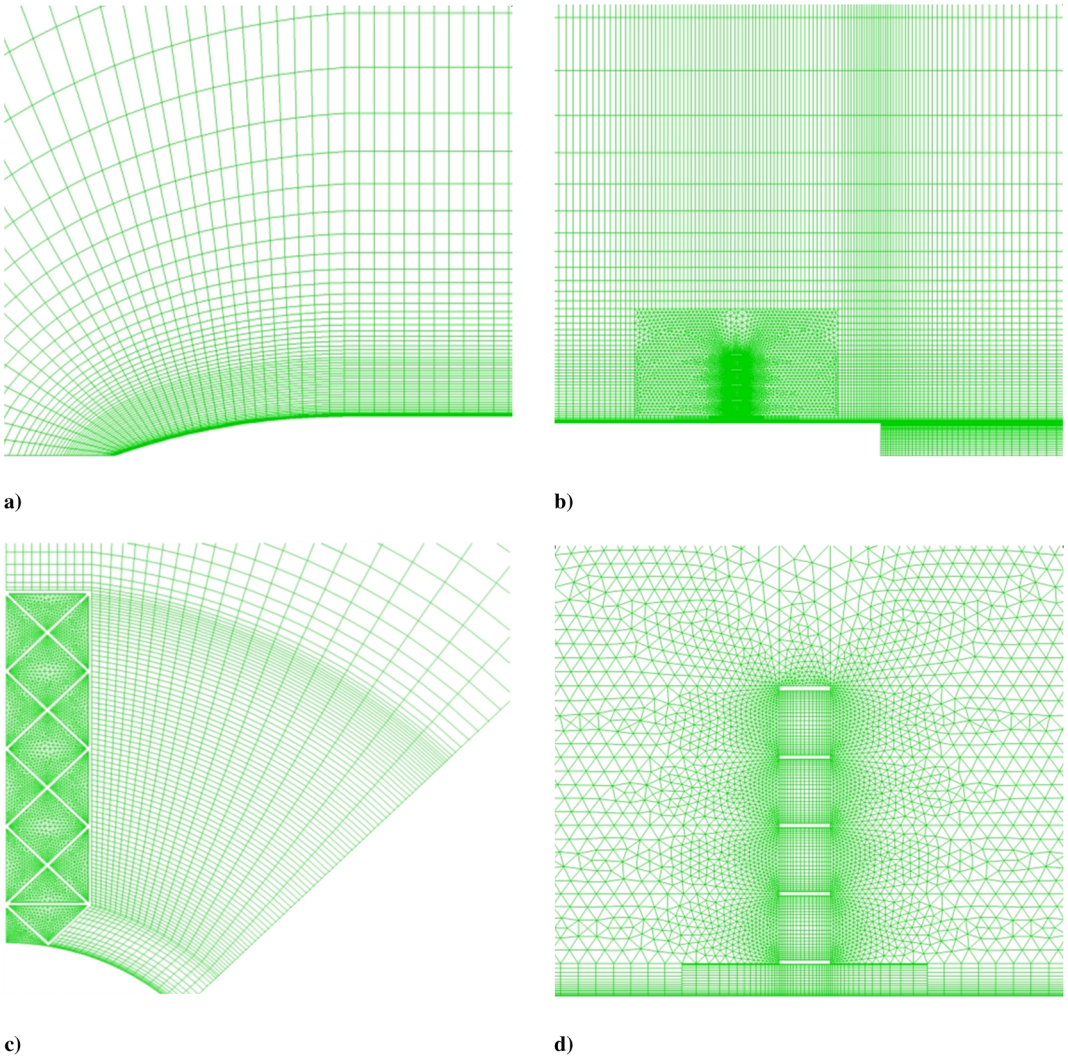

Fig. 2 Mesh topology for the missile with baseline grid fins: a) front nose region at the symmetry surface along the body axis, b) wake region at the symmetry surface along the body axis, c) fin surface perpendicular to the body axis, d) fin region at the symmetry surface along the body axis.

Table 1 Comparisons of the drag coefficient on the whole missile (C_D) with the drag coefficient on the grid fin only (C_{Df})

Freestream Mach number	Drag on baseline missile	Drag on baseline grid fin	Drag percentage on fin, %	Drag on amended missile	Drag on swept-back grid fin	Drag percentage on fin, %	Drag reduction on missile, %	Drag reduction on fin, %
0.905	0.784	0.504	64.29	0.734	0.437	59.53	6.38	13.29
1.045	0.922	0.448	48.59	0.870	0.392	45.06	5.64	12.50
1.190	0.896	0.406	45.31	0.856	0.353	41.24	4.46	13.05
1.332	0.841	0.384	45.66	0.796	0.332	41.71	5.35	13.54
2.0	0.700	0.345	49.29	0.662	0.302	45.62	5.43	12.46

For the swept-back grid fin, the grid topology is identical to that of the baseline grid fin and is omitted for the sake of brevity.

D. Boundary Conditions

The freestream Mach number ($M\infty$) is set at 0.817–2.0 and the Reynolds number (Re_D) is 4.69–11.48 $\times 10^5$ (based on diameter D) for comparison with the ARF free-flight test data. The freestream static pressure and temperature is 1 atm and 295 K, respectively. The angle of attack is 0. Far-field pressure boundary conditions were applied for the outer radial boundary; symmetric conditions for surfaces of symmetry, and nonslip conditions for all solid surfaces. At the downstream outflow boundary, a user-defined function is compiled to extrapolate all the flow quantities from the interior grid points.

III. Results and Discussions

A. Aerodynamic Axial Force

The aerodynamic drag coefficients (C_D), also called the axial force coefficients in body coordinates, are calculated using the FLUENT postprocessor to integrate the viscous and pressure forces on the body and fin surfaces. Figure 3 shows the drag coefficients of the present study compared with the ARF free-flight test results [6] and CFD results provided by Hughson et al. [12] under transonic and supersonic flow conditions at a freestream Mach number ($M\infty$) of 0.8–2.0 for the missile with baseline grid fins.

The trends of drag for all the data consistently show that the drag coefficient increases with an increase in Mach number for low transonic to sonic conditions; but with a further increase in Mach number to supersonic conditions, the drag coefficient decreases gradually. The increase in drag is explained in the literature to be a result of flow choking within the lattice grid cells under transonic conditions.

From Fig. 3, it is clearly shown that the present results agree well with the previous CFD results provided by Hughson et al. [12]. The good agreement indicates that the present numerical method is accurate enough to capture the flow physics over a missile attached with grid fins. The large deviation between the present CFD data and ARF free-flight test data [6] may be due to the differences in free-flight conditions at ARF and the flow conditions of the current study. Hughson et al. [12] indicated that a reasonable error estimate for the Mach number should be about $\pm 10\%$ in the transonic regime for the ARF free-flight test. They further reported that the total error estimate of forces was challenging to obtain because the aerodynamic coefficient data were extracted from the missile trajectory based on chronograph timings coupled with the position and orientation of the missile during its flight.

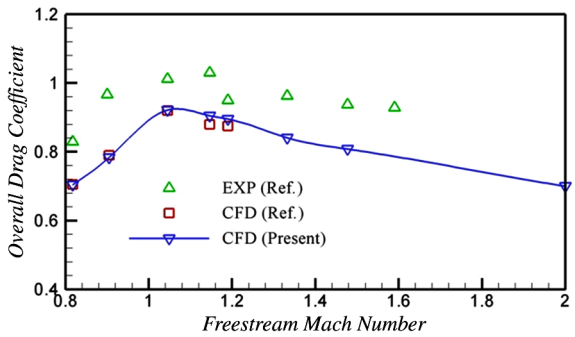

Fig. 3 Drag coefficient (C_D) on the whole missile with baseline grid fins versus freestream Mach number.

Next, the present numerical method is employed to simulate the flows over the missile with a swept-back grid-fin configuration in the transonic and supersonic regimes at Mach numbers of 0.8–2.0. Similarly, the aerodynamic drag coefficients are calculated for the whole missile configuration as well as the grid fin alone. Table 1 lists the drag coefficients (C_D) on the whole missile with grid fins and the drag coefficients (C_{Df}) on the grid fin alone.

The drag coefficient on the baseline grid fin and swept-back grid fin is largest at a transonic Mach number of 0.905 and decreases with increasing freestream Mach number. The reason is due to the strongest transonic flow choking within the grid-fin cells at this Mach number, which in turn leads to the highest drag coefficients on fins for both the baseline and swept-back models. How to overcome the flow choking and to reduce the high transonic drag is precisely the main objective of the present study. The percentage of the total drag accounted for by the grid fin alone is as high as 64.29% for the baseline grid fin and 59.53% for the swept-back grid fin at a subsonic Mach number of 0.905. It decreases suddenly to 48.59% for the baseline grid fin and 45.06% for the swept-back grid fin at a sonic Mach number of 1.045. This is followed by a moderate increase for a supersonic Mach number of 2.0. The drag on the ogive cylinder can be obtained by deducting the drag on the grid fin from the total drag. It is found that the drag on the ogive cylinder is almost unchanged when the baseline grid fin is replaced by the swept-back grid fin.

The data in Table 1 clearly shows that it is beneficial to use swept-back grid-fin configurations to achieve a reduction in drag. The drag drops by about 4.46–6.38% on the missile with swept-back grid fins for all Mach numbers investigated. When only the drag on the grid fin is considered, the drag reduction for the swept-back grid fin is about 12.46–13.54% compared with the baseline fin. This is believed to be due to the swept-back framework of the grid fin, which sets up an inclination between the oncoming flow and the fin cells. The "effective nozzle length" for each fin cell is reduced and the flow is allowed to pass over each of the adjoining cell spars locally and independently. Flow choking within the fin cells is thus reduced or avoided, as will be detailed in the subsequent section.

B. Flow Characteristics

According to the area–Mach number relation in a quasi-one-dimensional nozzle, subsonic flow will speed up while going through a converging nozzle. For a critical freestream Mach number, the flow reaches the sonic speed limit at the nozzle throat. This in turn limits the flow rate and causes the flow to "choke" within the nozzle. As such, the flow choking phenomenon can also be investigated by analyzing the Mach number distribution within the grid-fin cells. Figure 4 shows the Mach number (Ma) contours on the surface of symmetry at freestream Mach numbers of 0.905, 1.19, and 2.0 for both fin configurations.

For the baseline configuration, the growth of the boundary layer coupled with stagnated flow at the leading and trailing edge of each cell spar causes every cell within the grid fin to operate like a converging–diverging nozzle. At a Mach number of 0.905, as shown in Fig. 4a, a sonic Mach number distribution is found within the grid-

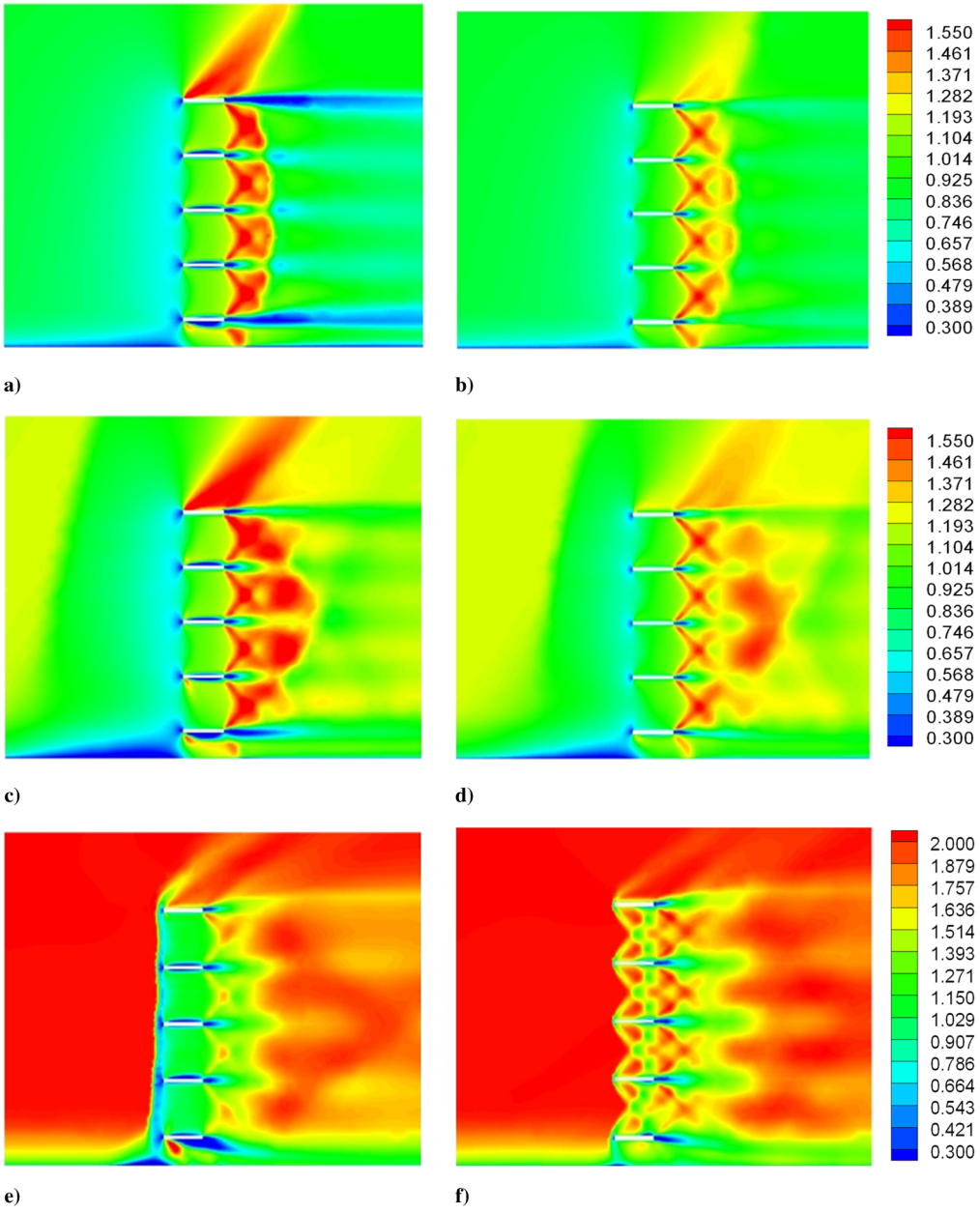

Fig. 4 Mach number contours on the surface of symmetry: a) baseline grid fin at freestream $M\infty = 0.905$, b) swept-back grid fin at freestream $M\infty = 0.905$, c) baseline grid fin at freestream $M\infty = 1.19$, d) swept-back grid fin at freestream $M\infty = 1.19$, e) baseline grid fin at freestream $M\infty = 2.0$, and f) swept-back grid fin at freestream $M\infty = 2.0$.

fin cells, indicative of choked flow within these cells. A three-dimensional diamond wave pattern is observed to develop in the region behind the lattice cells due to the interaction of the expansion wave generated at the cell exit.

When the Mach number is increased to 1.19, a weak compression shock forms just in front of the grid fin. Behind this compression shock, the flow is subsonic and the flow choking phenomena within the fin cells subsequently occurs (Fig. 4c). With a further increase in the Mach number to 2.0 (Fig. 4e), a strong normal shock wave similarly forms in front of the grid fin. Again, behind this normal shock the flow speed decreases and attains a subsonic value. The sonic flow speed distribution within the grid-fin cells indicates that the flow choking phenomena over the grid-fin cells is unchanged as in the aforementioned cases. Only when the freestream Mach number is increased further to 2.8, as shown by Hughson et al. [12], no normal shock is formed in the front of the grid fin, that is, the normal shock is "swallowed" by the fin cells, flow speed within the grid-fin cell is supersonic, and the flow is no longer choked.

As shown in Fig. 1b, the lattice geometry of the grid fin entails cubic and prismatic cells. For the swept-back grid fin, the framework of the fin is swept back along the chord direction by 30 deg; the cubic cells located within the middle of the fin are truncated and no longer act as "complete" nozzles as in the baseline fin. Flow passes over each of the adjoining cell spars of these cubic cells with less interaction. As shown in Figs. 4b, 4d, and 4f, it is observed that flow choking is reduced within the cubic cells. However, the prismatic cells located around the perimeter of the swept-back framework (see Fig. 1b) still appear to act as nozzles even though the inlet and outlet are inclined. The limit of 14% in terms of drag reduction on the grid fin may be due to the sustained presence of flow choking within these prismatic cells.

At $M\infty = 0.905$, the original three-dimensional diamond wave pattern behind the lattice cells of the baseline grid fin (Fig. 4a) is now reduced in Mach number magnitude and pattern area (Fig. 4b), indicating weaker expansion of the flow at the trailing edge of the cell spar for the swept-back grid fin. When the Mach number increases to

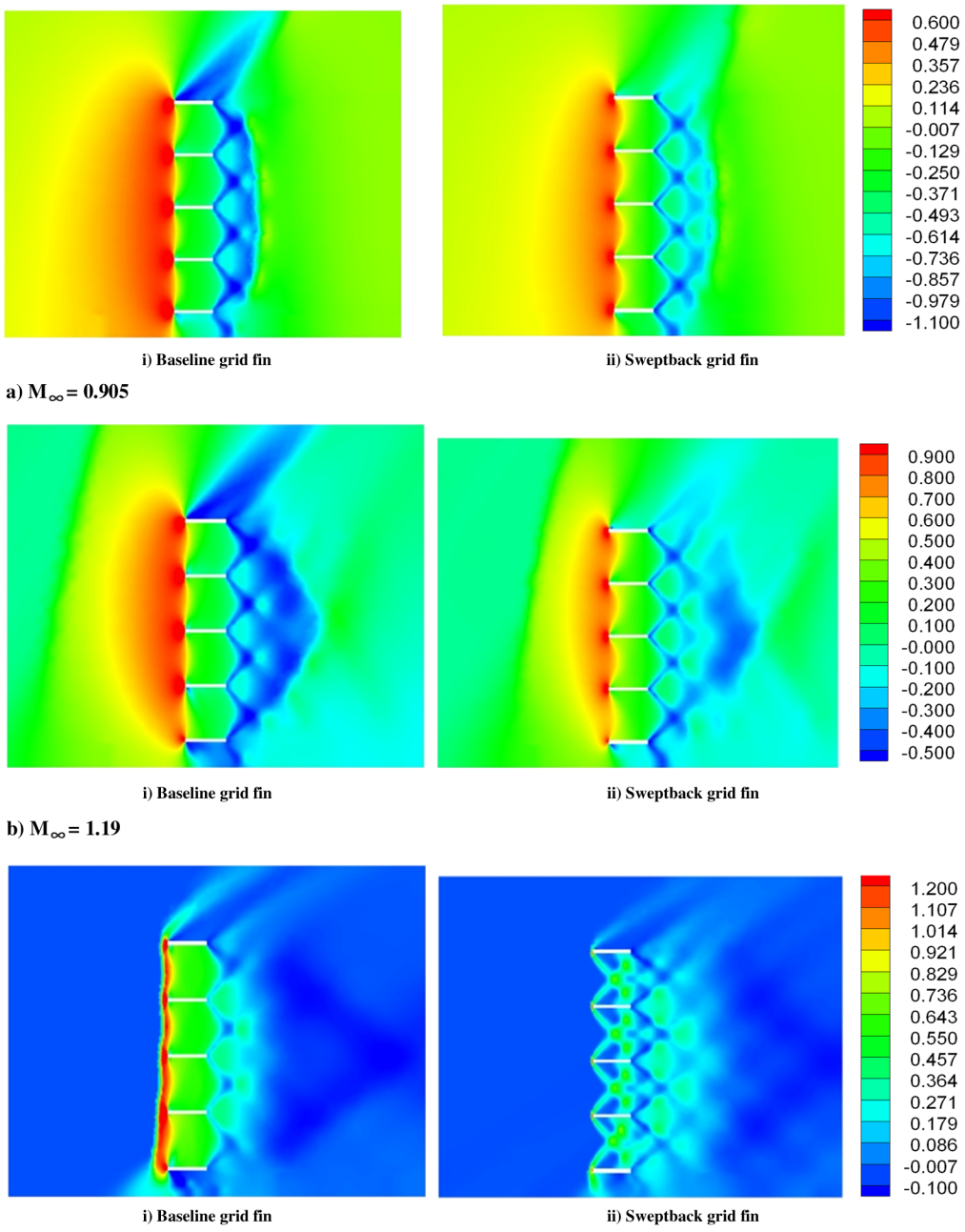

Fig. 5 Pressure coefficient contours for the baseline and swept-back grid fin on the surface of symmetry at freestream $M\infty = 0.905$, 1.19, and 2.

1.19, there is also a very weak compression shock wave formed upstream of the fin (Fig. 4d). It should be noted this weaker compression shock is located nearer to the leading edge of the fin compared with the baseline grid fin due to the weaker resistance. The flow pattern also shows the reduction in the expansion and interaction of the expansion wave behind the fin cells. These weaker expansions at the trailing edge of the cell spar indicate the lower flow resistance for the swept-back grid fin. When the Mach number is further increased to 2.0, the normal shocks that form immediately upstream of the fin in the previous cases are replaced by local oblique shock waves at the leading edge of the cell spar. The flow remains supersonic within the cells and an expansion wave forms at the trailing edge of the cell spar (Fig. 4f). Flow choking is notably absent.

The pressure coefficient (C_p) contours on the surface of symmetry are shown in Fig. 5. For a subsonic freestream Mach number of 0.905, flow stagnation at the blunt leading edges of each cell spar as well as flow choking within each of the cells causes a pressure increase in front of the fin. For supersonic freestream Mach numbers of 1.19 and 2.0, the pressure jump across a compression shock wave that forms in front of the fin further magnifies this pressure increase. A lower pressure distribution is also found within the base of the cell spar. The blunt trailing edge of each cell spar causes a rapid expansion of the supersonic flow leading to flow acceleration and a pressure decrease further behind the grid fin.

Through comparisons of the pressure coefficient contours for the baseline and swept-back grid fin, it is clearly seen that the pressure gradient is higher for the baseline grid-fin configuration. For the swept-back grid fin, the pressure in front of the fin is lower compared with the baseline fin and the weaker expansion at the trailing edge leads to a smaller pressure drop. In particular, for a Mach number of 2.0, the absence of the normal shock upstream of the grid fin and the reduction in flow choking within the cells results in an even smaller pressure gradient for the flow passing through the swept-back grid fin, implying a further reduction in drag.

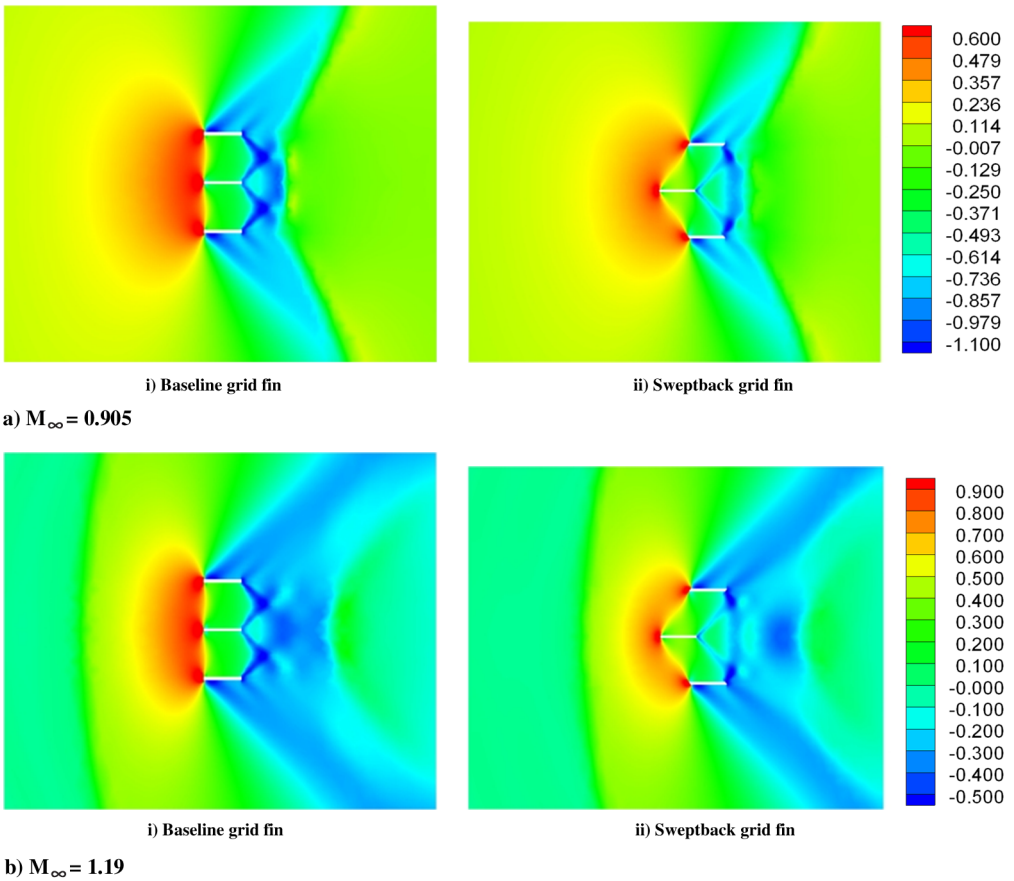

Fig. 6 Pressure coefficient contours for x–z slices passing through the middle of the rectangular grid-fin framework for the baseline and swept-back grid fin at freestream $M\infty = 0.905$ and 1.19.

Figure 6 shows the pressure coefficient contours on x–z slices passing through the middle of the rectangular framework for the baseline and swept-back grid fin at $M\infty = 0.905$ and 1.19, respectively. These two figures clearly show the same pressure distribution over the baseline and swept-back grid-fin configurations, further elucidating the favorable function of using swept-back grid fins to reduce flow resistance, flow choking, and, subsequently, drag force.

IV. Conclusions

The primary advantage of a grid fin as a less conventional missile tail control surface is the requirement of a smaller actuator to rotate it in a high-speed flow. Because of its shape and small chord length, another advantage of the grid fin is that it is more compact and can be made easier to store or transport by folding it against the adjoining body. However, the disadvantage of the grid fin is its relatively high drag within the transonic and low supersonic regimes.

Numerical studies have been conducted for the flowfields over a baseline missile–grid-fin combination with dimensions identical to that tested by Abate et al. [6] at ARF. The large deviation between the current numerical data and the ARF test data may be due to the differences in the free-flight conditions at ARF and the flow conditions used in the current study. Numerical results, which agree well with the CFD results obtained by Hughson et al. [12], indicate that the drag increase is due to flow choking within the grid-fin cells.

To reduce flow choking, an improved design, which is termed a swept-back grid fin, is proposed, which is believed to leave the control effectiveness of the grid fin almost unchanged. The framework of the baseline grid fin is swept back along the chordwise direction and the overall effect is that the cubic cells located within the middle of the grid fin no longer act as complete nozzles such as those formed by the baseline grid-fin cells. The present numerical simulations show that the choked flow can be reduced within these cubic cells, and this subsequently results in about a 13% drag reduction for the fin at various transonic and low supersonic Mach numbers. Further studies to reduce flow choking may continue to focus on the choice of swept-back angle as well as changing the geometry of the cells, because flow choking still occurs within the prismatic cells located around the perimeter of the swept-back frame. These prismatic cells continue to act as nozzles despite the imposed inclination in the inlet and outlet.

Acknowledgment

The authors would like to thank Chng Tat Loon for his help in revising this manuscript.

References

[1] Belotserkovskiy, S. M., Odnovol, L. A., Safin, Y. Z., Tyulenev, A. I., Frolov, V. P., and Shitov, V. A., "Wings with Internal Framework," Foreign Technology Division Machine Translation FTDID (RS) T 1289, Feb. 1987.

[2] Burkhalter, J. E., Hartfield, R. J., and Leleux, T. M., "Nonlinear Aerodynamic Analysis of Grid Fin Configuration," *Journal of Aircraft*, Vol. 32, No. 3, May–June 1995, pp. 547–554. doi:10.2514/3.46754

[3] Theerthamalai, P., and Nagarathinam, M., "Aerodynamic Analysis of Grid-Fin Configurations at Supersonic Speeds," *Journal of Spacecraft and Rockets*, Vol. 43, No. 4, 2006, pp. 750–756. doi:10.2514/1.16741

[4] Washington, D., Booth, P. F., and Miller, M. S., "Curvature and Leading Edge Sweep Back Effects on Grid Fin Aerodynamic Characteristics," AIAA Paper 93-3480, June 1993.

[5] Miller, M. S., and Washington, D., "An Experimental Investigation of Grid Fin Drag Reduction Techniques," AIAA Paper 94-1914, June 1994.

[6] Abate, G., Winchenbach, G., and Hathaway, W., "Transonic Aerodynamic and Scaling Issues for Lattice Fin Projectiles Tested in

a Ballistic Range," *Proceedings of the 19th International Symposium of Ballistics*, edited by I. R. Crewther, Vol. 1, Symposium Office, Thun, Switzerland, May 2001, pp. 413–420.

[7] Chen, S., Khalid, M., Xu, H., and Lesage, F., "A Comprehensive CFD Investigation of Grid Fins as Efficient Control Surface Devices," AIAA Paper 2000-987, Jan. 2000.

[8] Lin, H., Huang, J. C., and Chieng, C., "Navier–Stokes Computations for Body/Cruciform Grid Fin Configuration," *Journal of Spacecraft and Rockets*, Vol. 40, No. 1, 2003, pp. 30–38. doi:10.2514/2.3912

[9] DeSpirito, J., and Sahu, J., "Viscous CFD Calculations of Grid Fin Aerodynamics in the Supersonic Flow Regime," AIAA Paper 2001-257, Jan. 2001.

[10] DeSpirito, J., Edge, H. L., Weinacht, P., and Sahu, J., "Computational Fluid Dynamics Analysis of a Missile with Grid Fins," *Journal of Spacecraft and Rockets*, Vol. 38, No. 5, 2001, pp. 711–718. doi:10.2514/2.3756

[11] DeSpirito, J., Vaughn, M. E., and Washington, W. D., "Numerical Investigation of Canard-Controlled Missile with Planar and Grid Fins," *Journal of Spacecraft and Rockets*, Vol. 40, No. 3, 2003, pp. 363–370. doi:10.2514/2.3971

[12] Hughson, M. C., Blades, E. L., and Abate, G. L., "Transonic Aerodynamic Analysis of Lattice Grid Tail Fin Missiles," AIAA Paper 2006-3651, June 2006.

M. Costello
Associate Editor